ACS OMEGA

http://pubs.acs.org/journal/acsodf
Article

Two Different Responsive Organosilica Nanocarriers to Combine Chemo- and Immunotherapy against Cancer

Maria Sancho-Albero,*[,¶] Alessia Lucrezia Fenaroli,[¶] Mirco Scaccaglia, Cristina Matteo, Chiara Grasselli, Massimo Zucchetti, Roberta Frapolli, Claudia Nastasi,[●] and Luisa De Cola*[,●]

Cite This: *ACS Omega* 2024, 9, 41225−41235
Read Online

ACCESS | Metrics & More | Article Recommendations | Supporting Information

ABSTRACT: The combination of chemo- and immunotherapy was recently demonstrated to improve a patient's response to therapy, giving rise to an emerging cancer treatment known as chemoimmunotherapy (CIT). Despite the promising benefits of CIT, the most important challenges are (i) the simultaneous or time-controlled delivery of two drugs and (ii) the selective uptake into different cells for each of the drugs: cancer cells for the chemotherapeutic and macrophages for the immunostimulation actives. Herein, a delivery strategy based on morphologically different stimuli-responsive breakable organosilica nanocarriers is exploited to transport two distinct drugs in the different cells using different times of delivery. We employ stimulus-sensitive, PEGylated organosilica nanocages to encapsulate the chemotherapeutic agent doxorubicin, which is preferentially taken up by tumor cells vs macrophages. On the other hand, similar size mesoporous organosilica nanoparticles, preferentially internalized by macrophages, are filled with the immunostimulator resiquimod. The administration in a sequential manner of the two different nanocarriers allowed us to assess the integrated effect of the combined therapy versus treatment with a single drug. *In vitro* work clearly shows an important reduction of tumor cell viability when both chemo- and immunotherapeutic agents are delivered.

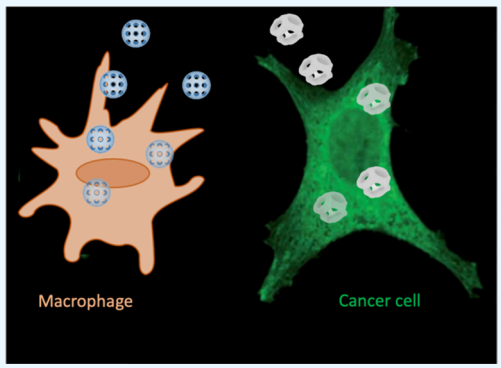

INTRODUCTION

Cancer is one of the most common causes of death worldwide, and in 2023 the number of new cancer cases reached 22 million.[1] Cancer is currently treated by local (such as surgery or radiation) or systemic therapies (chemotherapy, immunotherapy, or hormone therapy). However, resistance to the treatments and recurrence often occur, and complete remission still represents a challenge.[2] In order to improve the success rate while reducing side effects, novel strategies are pursued that include immunotherapy, targeted therapy, and precision medicine.[3,4] Also, recently the combination of chemotherapy and immunotherapy, originating as the so-called chemo-immunotherapy (CIT),[5,6] opened an innovative approach for cancer treatment that has significantly grown over the last years, with particular relevance in tumors resistant to first-line treatments.[7] This strategy induces both cancer cell death via the chemotherapeutic agent and stimulation of the immune system, boosting a specific antitumor response via an immunostimulant. The efficiency of this combination was recently demonstrated by the improvement in patient's response to therapy.[8−10]

However, despite its promising benefits, some challenges need to be overcome, such as 1) possible systemic toxicity of both therapeutic agents; 2) low solubility of the drugs that limit their administration;[9] and 3) chemotherapeutic molecules and immunotherapeutic drugs, which affect different cellular and molecular targets, with different mechanisms of action, and therefore selective delivery in the desired cells is required. A possible strategy to overcome some of the above-mentioned problems is the use of some kind of nanocarrier to improve the circulation time, to protect the drugs until they reach the target, and to find a formulation for the insoluble molecules. In addition, the simultaneous or time-controlled release of different drugs in different cell types would permit a synergic combination, resulting in a more efficient therapy.

Nanocarriers can indeed provide interesting and suitable materials that may provide possible solutions for the realization of efficient CIT.[10] Organic (such as liposomes, exosomes), polymeric, and inorganic (such as metallic or metal oxide) nanoparticles (NPs), as well as hydrogels and nanogels, have been developed as delivery systems for CIT.[11] Among them, the interest in silica NPs has been significantly increased during past decades, mainly due to their good physical−chemical

Received: March 24, 2024
Revised: July 22, 2024
Accepted: August 8, 2024
Published: September 25, 2024

properties, such as composition, controllable size, porous structure, morphology, high surface area, stability and biocompatibility, and feasibility of being functionalized.[12] For instance, Yang et al.[13] created a nanoreactor based on a hybrid silica framework with Cu^{2+} species and tetrasulfide groups to simultaneously trigger Fenton's reaction and GSH depletion, activating the immune system in doxorubicin (DOX) treated cells for concurrently enhanced CIT. Using a different approach, Liang et al. created hollow mesoporous silica NPs functionalized with interleukin-2 (IL-2) and coated with a lipid bilayer to coencapsulate a drug to stimulate the immune system, all-trans retinoic acid (ATRA), and the chemotherapeutic DOX, exhibiting a great synergy effect on inhibiting tumor growth.[14] Also, Qian et al. demonstrated that DOX-loaded mesoporous silica-zinc oxide (MS-Zn) microrosettes stimulated the immune responses of macrophages with the Zn ions and meanwhile caused cell death by the sustained release of the DOX against Lewis lung carcinoma.[15] In 2022, Feng et al. validated the synergistic effect of periodic mesoporous organosilica nanoparticles (PMOs) loaded with DOX and functionalized with the tumor necrosis factor-related apoptosis-inducing ligand (TARIL) as a targeting and therapeutic factor. The synergistic effect was demonstrated in terms of tumor death caused by apoptosis of cancer cells and by the activation of the immune response in breast cancer cells (MCF-7 and 4T1).[16] In a different work, Wang et al. reported a multifunctional and theragnostic silica nanoenzyme loaded with Cu@Fe_2C NPs and R848 and functionalized with PEG/LA, the nucleolin-specific aptamer AS1411, and the fluorescent dye ICG for real time imaging and synergistic cancer therapy.[17]

For any nanocarrier designed, degradation and complete elimination are a must to prevent accumulation of the nanomaterials, or their degradation products, in vital organs. In recent years several systems have been developed to obtain on demand breakable particles capable of releasing the drug encapsulated and, meanwhile, being eliminated from the organism.[18,19] In particular, breakable silica NPs have been obtained by inserting stimuli-responsive functional groups within the silica structure such as disulfide bonds. The S−S bonds can be broken to form thiols, SH, under reducing conditions (for instance, by glutathione (GSH) present in high concentration in cancer cells), leading to the degradation of the structure of the NP, which is fundamental both for the release of the entrapped drug and for their complete elimination from the body.[18,20−22]

Here we report a multicomponent chemoimmunotherapeutic system, based on organosilica breakable NPs, combining two different morphologies: a nanocage (ssOSCs) of about 20 nm that is able to escape macrophages filtering[19] and a mesoporous organosilica NP (ssMSN) of the same size, which is internalized massively by macrophages. The breakability of the structures is ensured by the insertion of disulfide groups in the silica network. Each type of NP has been loaded with a different drug: the anticancer DOX was placed in the ssOSCs and the immune response inducer Resiquimod (R848) in mesoporous silica. To enhance macrophage selectivity, non-PEGylated ssMSNs were used to deliver the immune response inducer. On the contrary, PEGylated organosilica nanocages (ssOSCs-PEG) were employed to target the cancer cells. We demonstrate the *in vitro* integrated action of the codelivery strategy, using the 4T1.2 and RAW-297 cell lines, improving the antitumoral effect compared to each single therapy. The findings of this study provide the design for an efficient chemoimmunotherapy approach against cancer, based on different morphologies and functionalization of organosilica breakable NPs.

EXPERIMENTAL SECTION

Materials. All chemicals were purchased from Merck and used as received. Sulfo-Cy5-NHS ester was acquired from Lumiprobe. Phalloidin-Alexa-568 and Hoechst 33342 were provided by Life Technologies.

Synthesis and Characterization of Silica Nanocarriers. Breakable organosilica nanocages (ssOSCs) were synthesized following a previously published protocol.[19,23,24] In brief, in a 100 mL ball flask equipped with a magnetic stirrer 408 mg (1.12 mmol) of cetrimonium bromide (CTAB) was dissolved in deionized water (50 mL) at 50 °C, while stirring for 30 min at 250 rpm. Then, aqueous NH_3 (12.5 μL, 28%) was added, and the stirring speed was increased to 750 rpm. Afterward, a mixture of tetraethyl orthosilicate (TEOS) (448.1 μL, 2 mmol) and (triethoxysilyl)propyl disulfide (BTDS) (102.8 μL, 0.223 mmol) was added, and the mixture was stirred for 20 h at 50 °C and 750 rpm.

The synthesis of breakable mesoporous silica nanoparticles (ssMSNs) was performed by dissolving CTAB (816 mg) in a solution of deionized water (100 mL) in a ball flask (250 mL). Then, the solution was heated to 50 °C and stirred (between 500 and 750 rpm) for 30 min, and 25 μL of aqueous NH_3 28%, followed by a mixture of 1 mL of TEOS and 241 μL of BTDS, was added consecutively into the solution. The mixture was stirred at 750 rpm for 20 h, at 50 °C.

In order to purify the NPs and to extract the CTAB out of the pores of the particles, both ssOSCs and ssMSNs were transferred into a dialysis membrane tube (Molecular Weight Cut off 10000) and dialyzed against EtOH/H_2O/AcOH (1:1:0.007 v/v/v) for 3 days and EtOH/H_2O (1:1 v/v) for 24 h. The particles were finally lyophilized, characterized, and then stored at 4 °C until use.

For internalization experiments, ssOSCs and ssMSNs were labeled with the sulfo-Cy5-NHS probe. A solution of sulfo-Cy5-NHS ester (0.5 mg, 0.643 μmol) in dry dimethyl sulfoxide (DMSO, 200 μL) was reacted with 3-aminopropyltriethoxysilane (APTES) (4.5 μL, 0.142 M in dry DMSO) under stirring for 30 min in the dark. The sulfo-Cy5-silane obtained was then added to the nanoparticles, and they were stirred overnight at room temperature.

The morphology of the synthesized NPs was assessed by TEM (T20-FEI Tecnai thermoionic TEM) operated at 200 kV with a LaB6 electron source fitted with a "SuperTwin" objective lens allowing a point-to-point resolution of 2.4 A. Particle solutions were pipetted into a TEM copper grid for imaging. The hydrodynamic diameter was measured using DLS, together with zeta potential analysis, and a Delsa Nano C Particle Analyzer (Beckman Coulter, operative wavelength 655 nm). The DLS measurements were performed on dispersions of the particles in deionized water. FTIR spectra were recorded with a Shimadzu IRAffinity-1 spectrometer. The attenuated total reflectance Fourier transform infrared (ATR-FTIR) spectra of the particle samples were collected using a spectral resolution of $\lambda = 4$ cm^{-1}, accumulating 45 scans from 600 to 4000 cm^{-1}, and the ATR-FTIR spectra were ATR corrected. TGA was finally conducted on a Netzsch model STA 449 fi Jupiter instrument. The samples (ca. 1 mg) were kept at 100 °C for 30 min for stabilization and then heated from 25 to 800

https://doi.org/10.1021/acsomega.4c02838
ACS Omega 2024, 9, 41225−41235

°C at a speed of 10 °C/min, before being held at this temperature for a further 30 min, and finally cooled. The analyses were performed under a 22 mL/min air flow. Powder X-ray diffraction (XRD) patterns were recorded by using a Bruker D2 Phaser diffractometer on lyophilized nanoparticle samples. The measurements were performed over a 2θ range from 10° to 60°, with a step size of 0.008°, resulting in a total of 6150 steps. Each step was measured for 0.25 s.

Resiquimod (R848) and DOX Loading into the NPs and Release. The loading of R848 in ssMSNs was achieved following an impregnation procedure in an EtOH/H_2O 1:0.1 ratio. In particular, 15 mg of ssMSNs and 3 mg of R848 were suspended in 900 μL of ethanol. Then, 100 μL of distilled H_2O was added to the mixture to favor the encapsulation of the drug within the NPs. Then, they were vigorously sonicated and mixed overnight at room temperature under orbital stirring. Subsequently, the sample was placed in a rotavapor at 40 °C until the solvent was completely evaporated. The NPs were then washed several times using a solution of H_2O/EtOH (7:3 v/v) to discard the nonencapsulated drug. The supernatant was then eliminated, and the final precipitate containing the ssMSNs with the encapsulated R848 (ssMSNs@R848) was resuspended in 0.5 mL of deionized water. ssMSN@R848 was thoroughly characterized by TEM, DLS, zeta potential, FTIR, and TGA. HPLC analysis, coupled to UV detection at 230 nm, was conducted to confirm and quantify encapsulated drug R848 in the inner cavity of the particles. For the encapsulation of DOX in ssOSCs, 5 mg of NPs and 1 mg of DOX were mixed in 1 mL of EtOH vigorously sonicated and left overnight at room temperature under orbital stirring and under darkness. Subsequently to force the encapsulation, the sample was placed in a rotavapor at 40 °C until the solvent was completely evaporated. The DOX-loaded ssOSCs (ssOSCs@DOX) were resuspended in 2 mL of H_2O and 80 μL of 3-[methoxy-(polyethyleneoxy)6−9]propyltrimethoxysilane, and 6−9 PE units were added to functionalize their surface and stirred for 3 h. Then, the water was eliminated again using the rotavapor and to remove the noninternalized DOX, and loaded NPs were washed with ethanol twice. The supernatant was then eliminated, and the precipitate containing the DOX-loaded and PEG-functionalized NPs (ssOSCS@DOX-PEG) was resuspended in 0.5 mL of deionized water. Since the DOX is a fluorescent drug, the emission spectrum of ssOSCs@DOX-PEG was recorded upon excitation at 490 nm (see Figure S1, SI) on a Horiba Jobin Yvon IBH FL-322 Fluorolog 3 spectrometer equipped with a 450 W xenon arc lamp, double grating excitation, and emission monochromators (2.1 nm/mm of dispersion; 1200 grooves per mm) and a TBX-04 single photon-counting detector. To estimate the loading of the entrapped drug, nanoparticles stored in water were broken by adding a solution of Glutathione, GSH, 10 mM in PBS (pH 7.4). After 24 h, the resulting solution was finally centrifuged to discard the broken particles, and the supernatant, containing the released drug, was analyzed. The encapsulation yield was determined using a calibration curve constructed by using different concentrations of DOX solutions and measuring the emission intensity for each solution. The concentrations of the DOX used for the calibration plot ranged from 0.97 μg/mL to 15.62 μg/mL DOX in distilled H_2O.

The drug release profile from both NP formulations was evaluated. Initially, 1.5 mL of the final solution of ssMSNs@R848 (R848: 231.8 μg/mL, loading 13%) and ssOSCs@DOX-PEG (DOX: 70.4 μg/mL, loading 3.5%), respectively, was diluted 1:5 with PBS. Then, 2 mL of the final solution was charged in a 3.5 MWCO membrane cassette (Thermo Fisher Scientific Inc., USA) and the dialysis performed at 37 °C against 600 mL of BSA, 40 mg/mL, in PBS. Aliquots were drawn after 15 and 30 min and 1, 2, 4.5, 6, and 24 h in order to establish the drug release. The experiment was repeated three times for each NP formulation.

Aberration corrected scanning transmission electron microscopy (Cs-corrected STEMHAADF) images were acquired using a high angle annular dark field detector in a FEI XFEG TITAN electron microscope operated at 300 kV equipped with a CETCOR Csprobe corrector from the CEOS Company allowing formation of an electron probe of 0.08 nm. Elemental analysis was carried out with an EDS (EDAX) detector, which allows performing EDS experiments in the scanning mode. Finally, to assess the stability of the nanoparticles (ssMSN@R848 and ssOSC@DOX-PEG) in terms of size and morphology, we utilized dynamic light scattering (DLS) and transmission electron microscopy (TEM). A suspension of the nanoparticles (0.05 mg/mL) was prepared in PBS and DMEM culture media and incubated at 37 °C with agitation. Samples were taken and analyzed using DLS every 24 h. Finally, TEM images were captured after 72 h of incubation to evaluate the morphology of the nanoparticles.

***In Vitro* Cellular Uptake and Cytotoxicity Studies.** B16-BL6 melanoma cells were grown in Minimum Essential Medium Eagle (MEM, Euroclone, Italy) supplemented with 10% fetal bovine serum (FBS, GIBCO, USA), 1% penicillin/streptomycin, 1% nonessential amino acids, 2% MEM vitamin solution, and 1% L-glutamine (Biowest, France). RAW-297 macrophages and 4T1.2 cells were cultured with Dulbecco's modified Eagle's medium (DMEM, GIBCO) complemented with 10% bovine serum (FBS, GIBCO) and 1% penicillin/streptomycin. Cells were maintained at 37 °C under the normoxic conditions.

Confocal microscopy (Nikon A1 confocal scan unit with a 100 × 1.49 NA oil immersion objective managed by NIS elements software) was carried out to evaluate cellular uptake and trafficking of cyanine 5, Cy5, and NPs labeled in the cells. In this case, the two cellular lines (B16-BL6 and RAW-297) were seeded at a density of 25×10^3 cells on 20 mm coverslips (placed in a 24-well plate) and allowed to grow for 24 h. Then, ssOSCs@DOX-PEG and ssMSNs@R848 (1 mg/mL of NPs: 15.85 μg DOX/mL) and 0.025 mg/mL of NPs (0.56 μg R848/mL) were resuspended in the adequate culture medium (described in the previous sections) and added to B16-BL6 and RAW-297 cells, respectively. The concentration range of NPs was chosen according to previous results published by our group.[19] They were then incubated for 2, 4, 6, 8, 24, 48, and 72 h. The internalization of ssOSCs in macrophage-like cells RAW-297 and the uptake kinetics of ssMSNs in B16-BL6 tumoral cells were also evaluated. Finally, cells were washed three times with PBS and fixed with 4% paraformaldehyde. Phalloidin-Alexa563 (Invitrogen) was used to label the cytoplasmic actin, and Hoechst was used to label the nuclei. NPs were functionalized with Cy5 in order to observe them by a confocal microscope at 650/670 nm excitation/emission wavelengths.

The cell's ability to uptake ssOSCs, ssOSCs-PEG, ssOSCs-NH_2, and ssMSN was also evaluated by flow cytometry at shorter time-incubation points using the empty NPs. Briefly, 25×10^3 cells (RAW-297, B16-BL6, and 4T1.2) were seeded onto a 24-well plate. Then, they were treated with Cy5-labeled

https://doi.org/10.1021/acsomega.4c02838
ACS Omega 2024, 9, 41225−41235

NPs (0.025 mg/mL of NPs), and at specific time points (2, 3, 5, and 24 h), cells were collected and analyzed by flow cytometry using a CytoflexLX instrument (Beckman Coulter). The data were analyzed by Kaluza Software 1.2 (Beckman Coulter). Nontreated cells were used to set the gate, and both the percentage of positive cells and the mean fluorescence intensity (MFI), assessed by geometric mean, were taken into account to assess nanoparticle internalization. For the detection of Cy5-labeled NPs, an excitation wavelength of 638 nm was used. The emitted signal was collected with BP 610/10 filters. All the samples were analyzed acquiring at least 10000 events.

***In Vitro* Coculture Assays: Evaluation of the Enhanced Therapeutic Effect against Breast Cancer Cells.** The antiproliferation activity of ssOSCs@DOX-PEG and ssMSN@R848 was tested using the MTT cell viability assay (ThermoFisher Scientific) on B16-BL6 and RAW-297, respectively. First, both cell lines were seeded onto a 96-multiwell plate at a density of 3×10^3 cells/well and were allowed to grow during 24 h. After that, ssOSCs and ssMSN were added to the cultures and incubated with the cells during 24, 48, and 72 h at different concentrations (from 0.0007 to 1 mg/mL of NPs and from 0.11 to 18.85 μg of DOX/mL and from 0.16 to 22.26 μg of R848/mL). After the incubation time points, cells were washed three times with PBS, and they were incubated with 10 μL of the MTT labeling reagent for 2 h following manufacturer instructions. Finally, 100 μL of the solubilization solution (HCl−isopropanol) was added and allowed to stand for 30 min. After complete solubilization of the purple formazan crystals, the absorbance of the samples was measured using a microplate reader (Infinite M200, TECAN). The wavelength used to measure the absorbance of the formazan product was 565 nm. Nontreated cells were used as negative controls (100% of viability). The viability of nonloaded nanoparticles (ssOSCs and ssMSNs) was also determined to confirm the effect of the encapsulated drugs. Experiments were done in triplicate, and the results are expressed as mean ± standard deviation. According to ISO 10993−5 (Biological evaluation of medical devices. Part 5: test for *in vitro* cytotoxicity) a reduction in cell viability higher than 30% compared to the control is considered as a cytotoxic effect.

To determine the efficacy of the codelivery CIT approach, a coculture system of breast cancer cells (4T1.2) and macrophages (RAW-297) was optimized. The coculture growing condition mimics the "tumor microenvironment", allowing us to better evaluate the antitumoral effects. In particular, after the optimization of the growing conditions of both cells in the 4T1.2 and RAW-297 coculture system, the evaluation of the cytotoxicity of ssOSCs@DOX-PEG and ssMSN@R848 was assessed using flow cytometry. First, 4T1.2 and RAW-297 were seeded onto a 24-multiwell plate at a density of 12×10^3 cells/well and 6×10^3 cells/well, respectively, and incubated for 24 h at 37 °C under normoxic conditions.

The ssMSN@R848 (0.075 mg/mL of NPs (1.67 μg R848/mL)) were added to the coculture and incubated for 24 h. Subsequently, the medium was collected and filtered before being added again to the coculture. Afterward, ssOSCs@DOX-PEG (0.001 mg/mL of NPs (0.016 μg DOX/mL)) was added. ssMSNs@R848 target macrophage-like cells to activate and stimulate the immune cells, and meanwhile, ssOSCs@DOX-PEG internalized in the breast cancer cells deliver the antitumoral drug DOX. The NPs were incubated with the cells during two time points (24 and 48 h), and after the incubation periods, cells were detached from the wells with trypsin and centrifuged for 5 min at 200*g*, and the supernatant was eliminated. For the evaluation of the cell viability and cytotoxicity by a flow cytometer, cells were suspended in blocking solution (PBS with 5% fetal bovine serum) at room temperature (RT) for 15 min. After centrifugation, cells were stained with mouse monoclonal APC-conjugated anti-CD45 (clone 30-F11, BioLegend, San Diego, CA, 1:100) for 20 min at 4 °C. Successively, cells were washed and stained with propidium iodide (Millipore, Burlington, MA, USA; 25 μg/mL). The samples were then immediately analyzed with a Cytoflex LX instrument equipped with CytExpert Acquisition software (Beckman Coulter, Miami, FL, USA); the acquisition process was stopped when 10,000 events were collected in the population gate. Offline analysis was performed using Kaluza 1.2 software (Beckman Coulter, Miami, FL, USA). A conventional gating strategy was used to remove aggregates and dead cells, and the anti-CD45 antibody was used to discriminate 4T1.2 cells from RAW-297 cells. For the detection of anti-CD45 and propidium iodide we used excitation wavelengths of 638 and 488 nm, respectively, and the emitted signal was collected with a 660/10 bandpass filter for anti-CD45 and with a 610/20 bandpass filter for propidium iodide.

The viability of 4T1.2 and RAW-297 cells was evaluated both in monoculture and in coculture conditions. Nontreated cells were used as negative controls (100% of viability). To determine that R848 molecules were not exhibiting any cytotoxic effect against the coculture, control cells treated with ssMSN@R848 but without ssOSCs@DOX were also analyzed under flow cytometry. In addition, with the aim to test the synergic effect of the coadministration of DOX and R848 released from the respective NPs, the proliferation of cells in a coculture system, treated only with ssOSCs@DOX but without ssMSN@R848, was also evaluated.

The therapeutic efficacy of the codelivery CIT approach was also validated using a coculture model composed by B16-BL6 and RAW-297 cells. First, B16-BL6 and RAW-297 were seeded onto a 24-multiwell plate at a density of 12×10^3 cells/well and 6×10^3 cells/well, respectively, and incubated for 24 h at 37 °C under normoxic conditions. The ssMSN@R848 (0.1 mg/mL) were added to the coculture and incubated for 24 h. Subsequently, the medium was collected and filtered before being added again to the coculture. Afterward, ssOSCs@DOX-PEG (0.02 mg/mL) were added. ssMSNs@R848 target macrophage-like cells to activate and stimulate the immune cells, and meanwhile, ssOSCs@DOX-PEG internalized in the cancer cells delivers the antitumoral drug DOX. The NPs were incubated with the cells during two time points (24 and 48 h). After the incubation periods, cells were detached from the wells with trypsin and centrifuged for 5 min at 200*g*, and the supernatant was eliminated. Finally, 1 mL of PBS and 10 μL of propidium iodide (25 μg/mL) were added to the precipitate, and cell viability was analyzed by flow cytometry. The viability of B16-BL6 and RAW-297 was evaluated both in monoculture and in coculture conditions. Nontreated cells were used as negative controls (100% of viability). To determine that R848 molecules were not exhibiting any cytotoxic effect against the coculture, control cells treated with ssMSN@R848 but without ssOSCs@DOX were also analyzed under flow cytometry. In addition, with the aim to test the synergic effect of the coadministration of DOX and R848 released from the, respective, NPs, the proliferation of cells in a coculture system,

https://doi.org/10.1021/acsomega.4c02838
ACS Omega 2024, 9, 41225−41235

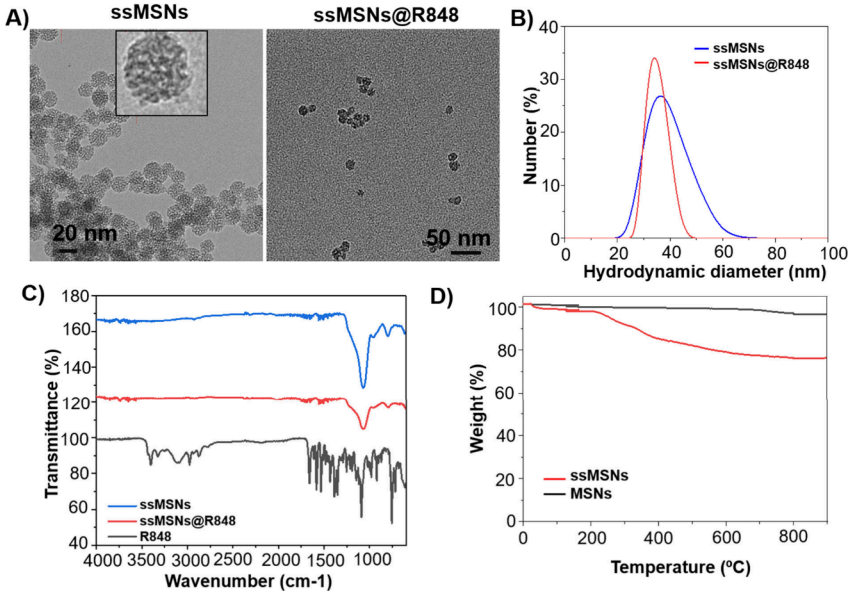

Figure 1. Characterization of ssMSNs and ssMSNs@R848. A) TEM images of empty and loaded NPs, B) Hydrodynamic diameter obtained by DLS, C) FTIR spectra of the drug (R848), the empty NPs, and the ssMSNs@R848, and D) TGA analysis of ssMSNs@R848.

treated only with ssOSCs@DOX but without ssMSN@R848, was also evaluated.

Statistical Analysis. The biological data were performed in triplicate. All the results are indicated as mean ± SD. Statistical analysis of the significant differences among the means were analyzed by two-way analysis of variance (ANOVA) for multiple comparisons by Dunnett's multiple comparisons test (GraphPad Software). Statistically significant differences were expressed as follows: $*p < 0.05$; $**p < 0.01$; $***p < 0.001$, and $****p < 0.0001$.

RESULTS AND DISCUSSION

Synthesis and Characterization of ssOSCs@DOX-PEG and ssMSNs@R848. The nanoparticles have been prepared as previously described,[18,19,22−24] and the details are reported in the experimental section. After purification, the nanomaterials have been characterized using TEM to determine their morphology and DLS and zeta potential for their hydrodynamic size, monodispersity, and surface charge. Electron microscopy images of empty ssMSNs and R848-loaded are depicted in Figure 1A. The particles were spherical in shape and clearly monodisperse with an average diameter of around 25−30 nm. DLS analysis of empty and loaded NPs shown in Figure 1B confirms the results of TEM analysis (NPs exhibited a hydrodynamic diameter around 30 nm). The zeta potentials of the ssMSNs and the ssMSNs@R848 were $\zeta = -25$ mV and $\zeta = -19$ mV, respectively.

The negative surface charge confirmed that the cationic surfactant (CTAB) was completely removed during the dialysis process and that the R848 molecule (which is positively charged) was successfully located and entrapped inside the ssMSNs rather than being attached to the surface of the particles. FTIR spectra (Figure 1C) revealed the presence of the characteristic peaks of the silica structure and the disulfide bond incorporated inside the framework of the NPs. In particular, the characteristic absorption bands at 1060 cm^{-1} correspond to the siloxane vibrations of $(SiO)_n$ groups, and the bands at 960 and 796 cm^{-1} were assigned to Si−O−Si stretching and Si−O−Si bending modes, respectively. The peaks at 2925 cm^{-1} and 2860 cm^{-1} were attributed to the S−S moieties. The TGA analysis of ssMSN showed a loss of 20% in weight that corresponds to the presence of the disulfide groups that provide the NPs with the breakability behavior. Finally, HPLC analysis allowed the quantification of the drug encapsulated in NPs that resulted in a concentration of R848 equal to 0.68 mg/mL, indicating that the encapsulation yield was 11% (22.26 μg of R848/mg of NPs). The release profile over time of R848 from ssMSNs@R848 was evaluated by dialysis against BSA (40% in PBS) at 37 °C. 50% of the drug is released after 6 h, while at 24 h the percentage of release reaches 83%.

In the case of ssOSCs@DOX-PEG, TEM images revealed the typical cage-like morphology with a size of 20 nm (PDI: 0.326). (Figure 2A). DLS measurements of empty and DOX-loaded ssOSCs confirmed the results obtained by electron microscopy, providing a hydrodynamic diameter of approximately 40 nm (Figure 2B). The surface charge of the ssOSCs-PEG and ssOSCs@DOX-PEG was −14 and −18 mV, respectively.

As in the case of the ssMSNs previously described, FTIR spectra (Figure 2C) revealed the presence of the characteristic peaks of silica and a disulfide bond incorporated inside the silica framework. Also, the characteristic peaks coming from the DOX molecules were observed in the FTIR spectra of ssOSCs@DOX, demonstrating its successful encapsulation.

When carrying out the TGA analysis of ssOSCs (Figure 2D) a weight loss of approximately 20% was observed and attributed to the disulfide groups present in the silica framework of the NPs. The analysis of the weight loss for ssOSCs@DOX-PEG revealed a mass decrease of approximately 50%, indicating that 30% of the sample mass corresponds to the polyethyleneglycols grafted on the nanoparticle surface and on the drug.

To estimate the amount of drug inside the nanocages, a comparison of the emission intensity of the DOX, before and after its release from the broken nanocarriers, was made, as shown in Figure 2E. The large increase of the emission signal after 24 h exposure to a solution of the reducing GSH agent,

https://doi.org/10.1021/acsomega.4c02838
ACS Omega 2024, 9, 41225−41235

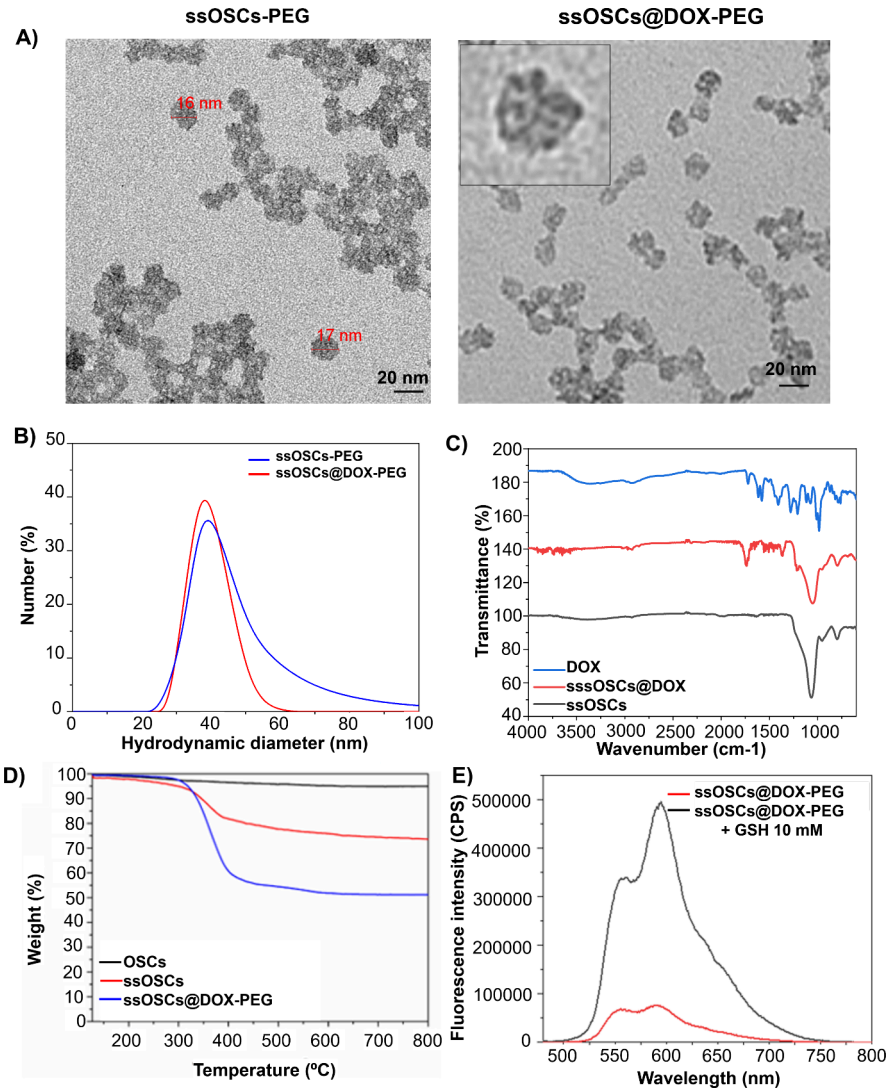

Figure 2. Characterization of ssOSCs and ssOSCs@DOX. A) TEM images of empty and loaded NPs, B) Hydrodynamic diameter obtained by DLS, C) FTIR spectra of the drug (DOX), the empty NPs, and the ssOSCs@DOX, D) TGA analysis, and E) Emission spectra of DOX before (red line) and after release (black line) from broken ssOSCs@DOX-PEG due to the presence of GSH (λ_{ex} = 490 nm).

proved that the DOX is released due to the reduction of the S−S bonds and the destruction of the silica structure. In order to quantify the amount of DOX entrapped inside ssOSCs, a calibration curve for the DOX was performed recording emission spectra at 7 different concentrations (from 0.97 to 15.62 μg/mL) of DOX in H_2O (Figure S1, Supporting Information). The concentration of the loaded DOX within the NPs was 15.9 μg of DOX/mg NPs.

The release profile of DOX from ssOSCs@DOX-PEG was evaluated by dialysis against BSA (40% in PBS) at 37 °C. Drug release amounted to percentages of 30% and 87% at 6 and 24 h, respectively.

Energy-dispersive X-ray spectroscopy (EDS) analysis (Figure S2) confirmed the presence of Si and S in the framework of both synthesized NPs loaded with the drugs (ssMSNs@R848 and ssOSCs@DOX-PEG). Furthermore, Figure S3, Supporting Information, indicates the formation of ssOSCs and ssMNSs with amorphous properties. The powder diffraction pattern evidences a broad peak at 2Θ around 22°, corresponding with the amorphous nature of the ssMSNs and ssOSCs. No ordered crystalline structure was observed.

Finally, the stability of both ssMSNs@R848 and ssOSCs@DOX-PEG was assessed in PBS and in cell culture media (DMEM). Figure S4 demonstrated that both types of loaded NPs maintained their particle size and morphology after 72 h incubation in both solvents under physiological conditions.

***In Vitro* Cellular Uptake and Cytotoxic Activity of Drug-Loaded NPs.** To assess the biological behavior and demonstrate the synergic effect of the proposed loaded nanoparticles in view of a possible therapeutic perspective, it is essential to understand the interactions between the particles and the target cells and how these interactions determine their cellular uptake. Confocal microscopy was employed to evaluate the cellular uptake and trafficking of ssOSCs@DOX-PEG and ssMSN@R848 in the B16-BL6 cells and RAW-297 macrophages, respectively. For internalization studies the nanoparticles were labeled with sulfo-Cy5. Cell cytoplasm was labeled using Phalloidin-Alexa568 and observed in green, and the nuclei were stained with Hoechst 33342 and observed in the blue region. Figure 3 shows orthogonal projections of the

https://doi.org/10.1021/acsomega.4c02838
ACS Omega 2024, 9, 41225−41235

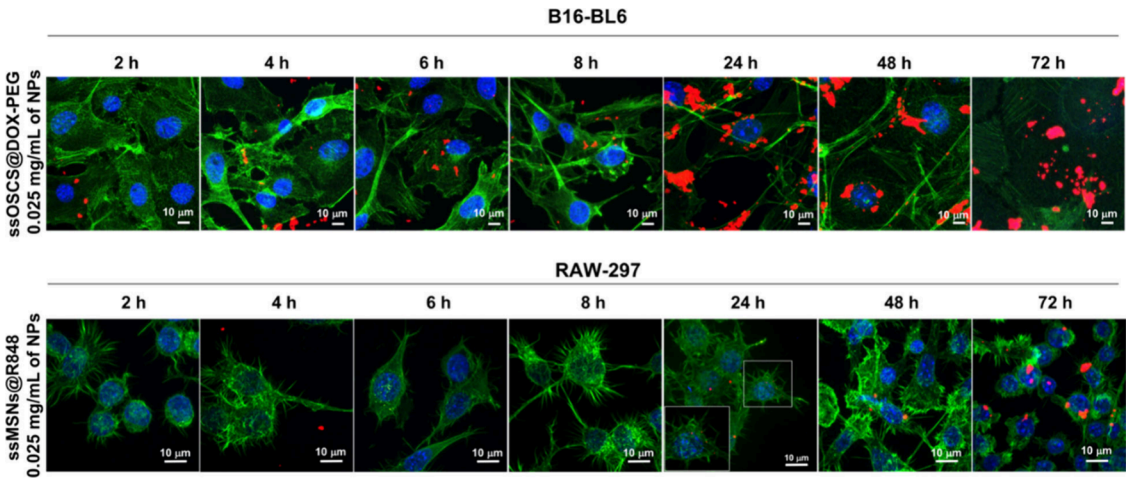

Figure 3. Internalization and uptake kinetics. Internalization of ssOSCS@DOX-PEG in B16-BL6 melanoma cells and uptake of ssMSNs@R848 by RAW-297 macrophages. Green: actin, blue: nuclei, and red: NPs.

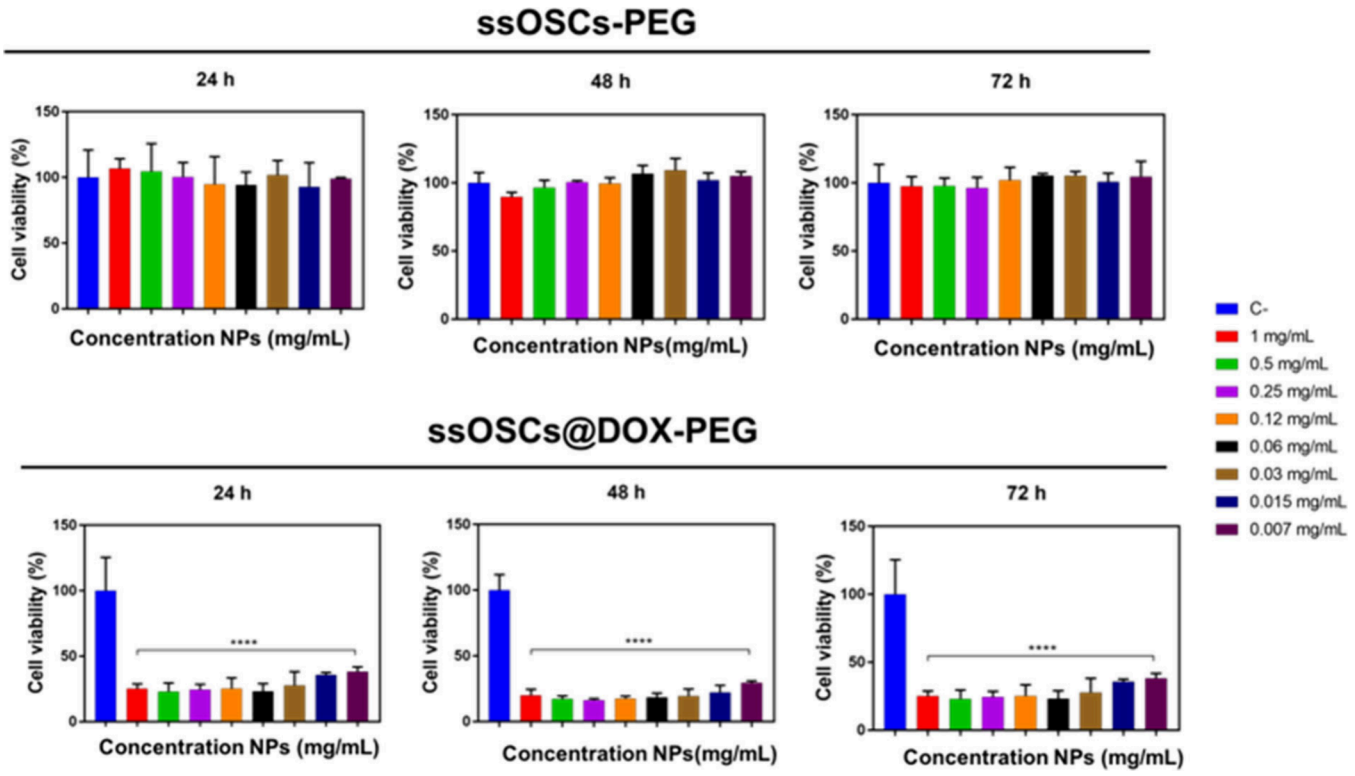

Figure 4. Cytotoxicity of ssOSCs@DOX-PEG evaluated by MTT in melanoma B16-BL6 cells. Empty ssOSCs: 0.007 to 1 mg/mL of NPs (from 0.11 to 18.85 μg of DOX/mL).

uptake of ssMSN@R848 (0.025 mg/mL of NPs (0.40 μg R848/mL)) by RAW-297 macrophages and of ssOSCs@DOX (0.025 mg/mL, of NPs (0.56 μg DOX/mL)) in B16-BL6 melanoma cells. In both cell lines, NPs were clearly internalized. Figure S5 includes confocal images of RAW-297 macrophage-like cells incubated with ssOSCs@DOX-PEG and B16-BL6 cells incubated with ssMSN@R848 molecules.

Confocal analysis confirmed that the presence of PEG on the surface of the nanocages enhances their cell uptake kinetics in cancer cells compared to macrophages. In fact, it is well-known that the presence of PEG molecules on surface NPs, besides improving their water solubility and avoiding their aggregation, disfavors the uptake from the macrophage.[25] We have indeed previously demonstrated that this cage-like morphology of ssOSCs minimizes their capture by immune cells.[19] Therefore, ssOSCs loaded with the chemotherapeutic drug DOX and functionalized with PEG tend to accumulate mostly in cancer cells, while the ssMSNs are efficiently filtered by the macrophage stimulation, upon release of R848, the immune response.

Flow cytometry results show the internalization of ssOSCs (Figure S6A), ssOSCs-PEG (Figure S6B), ssOSCs-NH_2 (Figure S6C), and ssMSN (Figure S6D). These results confirm again that the presence of the PEG around the NPs contributes to the decrease of their internalization by macrophages and, at the same time, favors the uptake of the

https://doi.org/10.1021/acsomega.4c02838
ACS Omega 2024, 9, 41225−41235

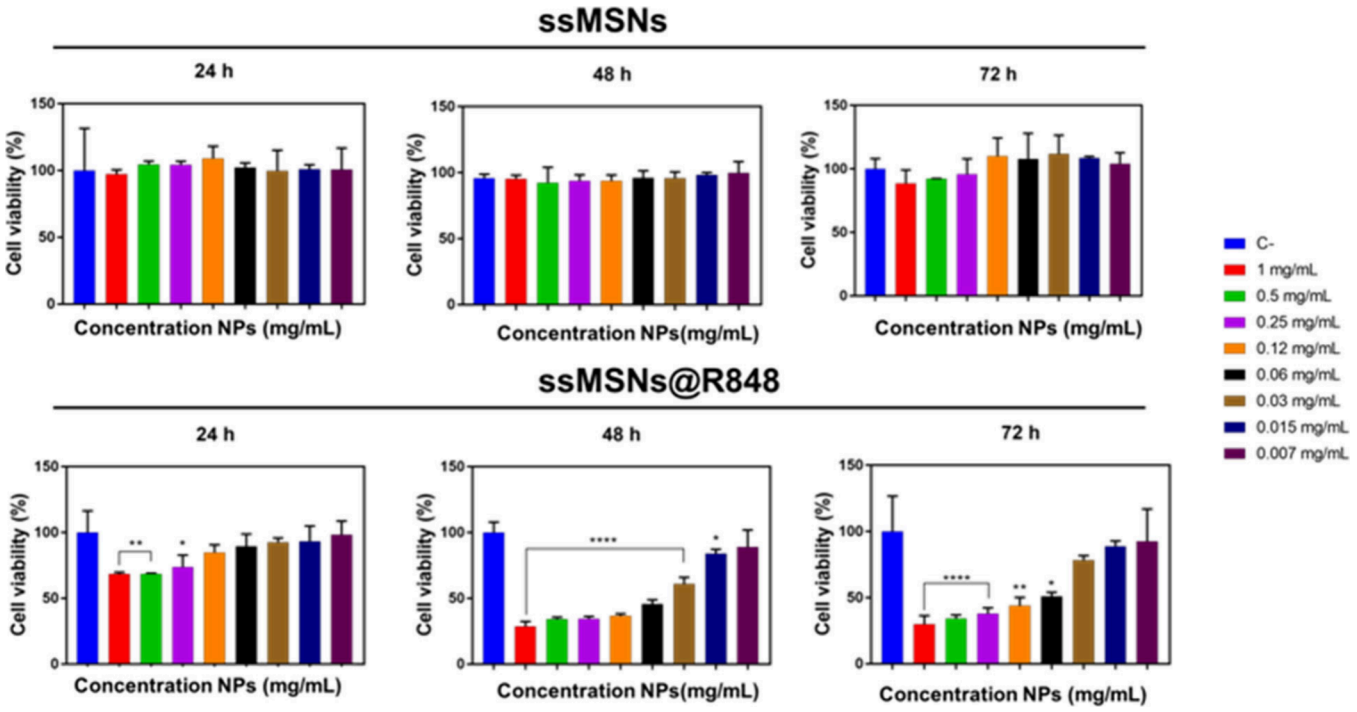

Figure 5. Tolerability of ssMSNs@R848 evaluated by MTT in RAW-297 macrophages. Empty ssMSNs were used as a negative control. NPs were incubated with the cells during 24, 48, and 72 h at a concentration range from 1 to 0.007 mg/mL of NPs (from 0.16 to 22.26 μg R848/mL).

NPs in the cancer cell line. To evaluate the effect of the NP surface charge, ssOSCs-NH_2 uptake kinetics were also studied. Investigation of these positively charged nanoparticles demonstrates that cage-like NPs were taken in larger amount by cancer cells (compared to macrophages) and that the positive charge, induced by the protonated amino groups present on the surface of the NPs, increases their cell internalization. These findings are in agreement with previous works that demonstrated a quicker and higher internalization kinetics when NPs are positively functionalized.[26,27]

To first verify the antitumoral activity of ssOSCs@DOX-PEG, the cell viability was evaluated on B16-BL6 melanoma cells. The tolerability of the tested cells to the exposure of the NPs was determined by incubating increasing quantities of the NPs (from 0.007 to 1 mg/mL of NPs; from 0.11 to 18.85 μg DOX/mL) for 24, 48, and 72 h. Empty NPs were also tested as a negative control to corroborate the absence of toxicity of the nanomaterial. The cytotoxicity assay revealed that empty ssOSCs-PEG induce no effects on cells, even at the highest dose during the last time point tested (Figure 4).

On the contrary, ssOSCS@DOX-PEG induced significant mortality on the cancer cells even at the lowest tested dose after only 24 h. These results confirm that DOX is able to be released from the breakable ssOSCs and inhibit the proliferation of cancer cells finally leading to cellular death. In the case of ssMSN@R848, their tolerance was determined on RAW-297 macrophages. Again, the viability of the cells was evaluated by using both empty and R848-loaded ssMSNs. Figure 5 shows the MTT results of RAW-297 exposed to ssMSN@R848 and ssMSN (from 0.007 to 1 mg/mL; from 0.16 to 22.26 μg R848/mL) for 24, 48, and 72 h. First, nonloaded ssMSNs were not toxic to the cells at any of the tested doses even after 72 h of incubation. On the contrary, the amount of ssMSN@R848 significantly reduced the viability of the macrophages in a concentration- and time-dependent way. From this experiment we found the appropriate dose of ssMSN@R848 necessary for stimulating the macrophage cell line to induce an immunomodulatory effect, but in the absence of toxicity.[28,29] Thus, the maximum dose of R848 was established to be 0.12 mg/mL, well tolerated by RAW-297 cell lines, allowing the action of the drug itself is to shift their phenotype from M0 or M2 to the immunostimulant M1. The reprogramming of the macrophage causes a secretion of cytokines that can trigger the immune system to attack cancer cells (as supported by current knowledge and preliminary data, here not shown).[30,31] The immunostimulant activity of the ssMSN@R848 was also confirmed by a pilot experiment where primary M0 and M2 derived by murine bone marrow were exposed to the loaded NPs; we observed a massive upregulation of genes M1-like (*nos2*, *il6*, *il12b*) compared to several controls confirming the macrophage activation (Figure S7).

***In Vitro* Coculture Assays: Evaluation of the Enhanced Therapeutic Effect against Breast Cancer Cells.** After preliminary internalization and cytotoxicity studies on individual cell line cultures, the combined action of the two drugs, R848 and DOX, was evaluated on a coculture system composed of tumoral 4T1.2 cells and RAW-297 macrophages. To demonstrate the potential and feasible application of the proposed CIT codelivery strategy herein developed, breast cancer cells were chosen as DOX is usually used against breast cancer in clinic.[32,33] Flow cytometry studies were carried out to determine the effect of administration of the treatment. In particular, cells were treated for 24 h with ssMSN@R848 (0.075 mg/mL of NPs (1.67 μg R848/mL)) to stimulate macrophages to release cytokines and inflammation factors. Then the growth medium was filtered to eliminate the ssMSN but maintained the proinflammatory factors released to the environment. This media was then complemented with ssOSCs@DOX-PEG (0.001 mg/mL of NPs (0.015 μg

https://doi.org/10.1021/acsomega.4c02838
ACS Omega 2024, 9, 41225−41235

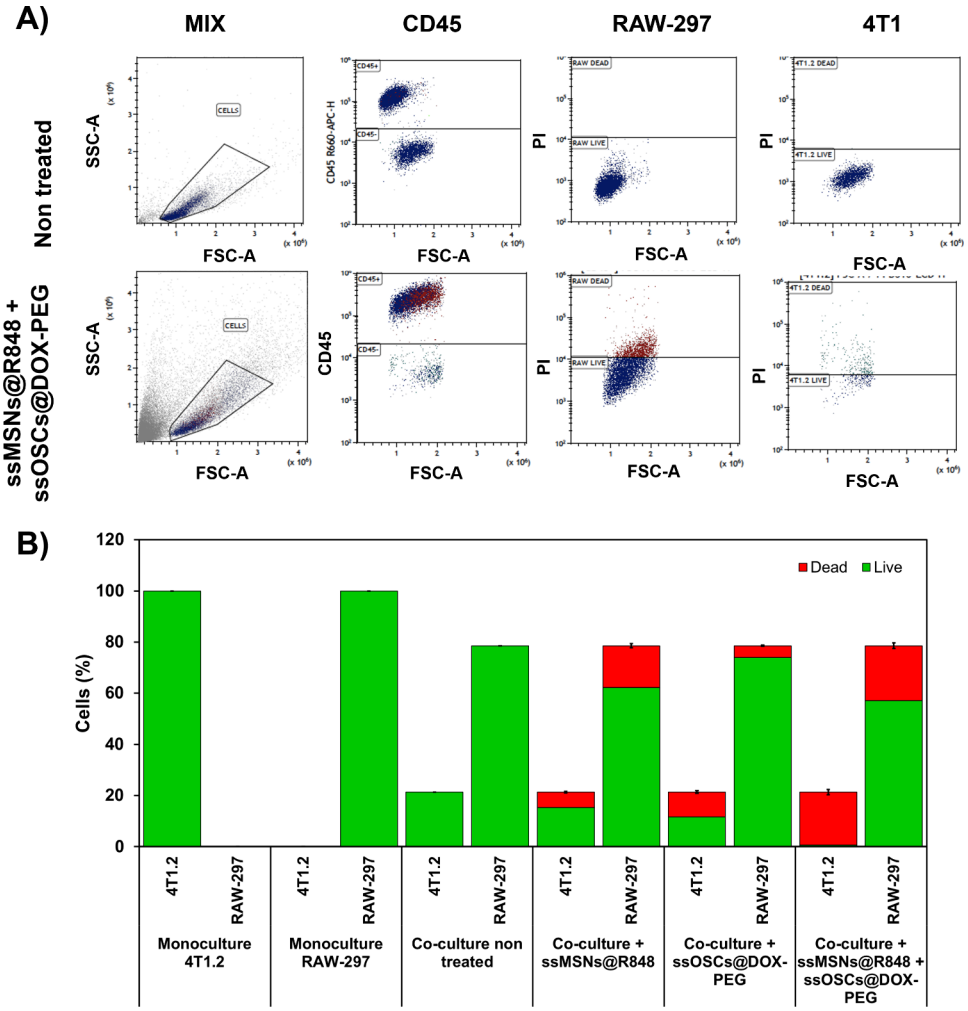

Figure 6. Flow cytometry analysis in cocultures treated with ssOSCs@DOX-PEG and ssMSN@R848 in a coculture of 4T1.2 and RAW-297. A) Flow cytometry dot plots of cocultures containing 4T1.2 and RAW-297 cells (the first line represents the control of nontreated cocultures). B) Analysis of the viability of both cell lines present in the cocultures demonstrating the enhanced cytotoxicity obtained with the chemoimmunotherapy mediated by the codelivery strategy of drugs entrapped in the different silica carriers.

DOX/mL)) and incubated again with the cocultured cells for a further 48 h. The proliferation and viability of 1) an independent culture of 4T1.2 cells; 2) an independent culture of RAW297 macrophages; and 3) a nontreated coculture were also assessed as controls. In addition. a coculture treated only with ssMSN@R848 and a coculture treated only with ssOSCs@DOX-PEG were studied. Flow cytometry results of cell viability in the cocultures are shown in Table S1 and Figure 6. As expected, untreated cells presented 100% viability in both monoculture and coculture. Also, the coculture treated for 24 h with ssMSN@R848 (0.075 mg/mL of NPs (1.67 μg R848/mL)) showed a viability of 71.7% (breast cancer cells) and 79.2% (macrophages), confirming that R848 at the concentration tested does not have a significant toxic effect on treated cells. When the cocultures were treated with ssOSCs@DOX-PEG (0.001 mg/mL of NPs), the viability of the cancer cells and the macrophages was 54.7% and 94.2%, respectively. Interestingly, in the coculture treated with both formulations, ssOSCs@DOX-PEG and ssMSN@R848, breast cancer cells exhibited a more pronounced cell mortality, decreasing to 3% of cell viability. The viability of macrophages of the treated coculture was not significantly affected, and the observed viability percentages were similar to the control coculture treated with only ssMSN@R848. These results confirm the improved combinatory cytotoxicity action of the two encapsulated drugs (DOX and R848 in ssOSC-PEG and ssMSN, respectively), leading to a significant reduction of cell viability and superior anticancer action compared with the single delivery approaches. They confirmed how the delivery of ssOSCs@DOX-PEG combined with ssMSNs@R848 significantly decreases the proliferation of breast cancer cells (i.e., activating immune cells), thus enhancing the potential therapeutic antitumoral action (compared with ssOSCs@DOX-PEG alone).

These results were finally validated in a second coculture model using B16-BL6 cells (Figure S8). The proliferation and viability of 1) an independent culture of B16-BL6 cells; 2) an independent culture of RAW297 macrophages; and 3) a nontreated coculture were also assed as controls. Also, a coculture treated only with ssMSN@R848 and a coculture treated only with ssOSCs@DOX-PEG were studied. Again, untreated cells presented 100% viability in both monoculture and coculture. Also, the coculture treated for 24 h with ssMSN@R848 (0.12 mg/mL) showed a viability of 100%, confirming that R848 at the concentration tested does not have a toxic effect on treated cells. In the case of the coculture

https://doi.org/10.1021/acsomega.4c02838
ACS Omega 2024, 9, 41225−41235

treated with ssOSCs@DOX-PEG, the viability of B16-BL6 tumoral cells was reduced only to 80%. On the contrary, the ssOSCs@DOX-PEG did not exhibit any toxicity against RAW-297 cells, but more interestingly, the coculture that was treated with the codelivery formulation of ssOSCs@DOX-PEG and ssMSN@R848 exhibited a more pronounced cell viability decrease. The reduction in cytotoxicity was marked for cancer cells. These data confirm again how the delivery of ssOSCs@DOX-PEG combined with ssMSNs@R848 significantly decreases the proliferation of cancer cells (i.e., activating immune cells), thus enhancing the potential therapeutic antitumoral action (compared with ssOSCs@DOX-PEG alone). These data confirm again how the delivery of ssOSCs@DOX-PEG combined with ssMSNs@R848 significantly decreases the proliferation of cancer cells (i.e., activating immune cells), thus enhancing the potential therapeutic antitumoral action (compared with ssOSCs@DOX-PEG alone).

CONCLUSIONS

Cancer is one of the main causes of death all over the world and is a multifaceted global health issue that continues to demand new solutions. In the last years, the combination of chemotherapy and immunotherapy has demonstrated the improvement in a patient's response to therapy, giving rise to an emerging strategy known as CIT. However, despite the promising CIT benefits, some challenges regarding the codelivery of the two agents remain, preventing a full translation to the clinic. As a result, drug delivery carriers ensuring effective and sustained drug release with improved therapeutic efficacy are urgently needed. The main difficulties are related to the use of different systems (chemical composition, size, surface functionalization) to address the different cells. In this work, we propose a new codelivery strategy based on the same type of nanoparticles, possessing the same chemical composition but different morphology and functionalization, to achieve selective internalization in macrophages and in cancer cells. In particular, we showed that the chemotherapeutic drug (DOX) encapsulated in nanocages, ssOSCs functionalized with polyethylene glycol, can kill cancer cells, while the immunostimulatory molecules (R848) are delivered in macrophages using mesoporous nanoparticle ssMSNs of identical size. This work is a preliminary study that validates the advantages of this combinatorial strategy in two coculture models of breast cancer cells with macrophages and of melanoma cells with macrophages, opening interesting possibilities for the development of multidelivery systems. Although future research with *in vivo* animal models is needed, this proof of concept demonstrates how the modulation of the employed materials can potentially serve to vehicle different drugs targeting specific cell lines for maximizing their therapeutic efficacy. However, it is still challenging to control the time for the different modes of action of the NP formulations since the activation of the immune system by the drug encapsulated in the MSNs should occur before the chemotherapeutic is released from the other NPs.

ASSOCIATED CONTENT

Supporting Information

The Supporting Information is available free of charge at https://pubs.acs.org/doi/10.1021/acsomega.4c02838.

Additional experimental results containing characterization and stability studies of the ssMSNs@R848 and ssOSCs@DOX, uptake kinetics evaluated by confocal microscopy and flow cytometry, gene expression analysis by real-time PCRs of bone-marrow-derived murine macrophages, and flow cytometry results of cocultures of B16-BL6 and RAW-297 treated with ssOSCs@DOX-PEG and ssMSN@R848 (PDF)

AUTHOR INFORMATION

Corresponding Authors

Maria Sancho-Albero − *Department of Biochemistry and Molecular Pharmacology, Istituto di Ricerche Farmacologiche Mario Negri, IRCCS, Milan 20156, Italy;* Present Address: Instituto de Nanociencia y Materiales de Aragón (INMA) CSIC-Universidad de Zaragoza, Campus Rio Ebro, Edificio I+D, C/Poeta Mariano Esquillor, s/n, 50018 Zaragoza, Spain. Networking Res. Center in Biomaterials, Bioengineering and Nanomedicine (CIBER-BBN), Instituto de Salud Carlos III, 28029 Madrid, Spain. Department of Chemical and Environmental Engineering, University of Zaragoza, Campus Rio Ebro, C/María de Luna, 3, 50018 Zaragoza, Spain. Instituto de Investigaciones Sanitarias de Aragón (IIS Aragón), 50009 Zaragoza, Spain; orcid.org/0000-0001-8762-5457; Email: msancho@unizar.es

Luisa De Cola − *Department of Pharmaceutical Science, DISFARM, Università degli Studi di Milano, Milan 20133, Italy; Department of Biochemistry and Molecular Pharmacology, Istituto di Ricerche Farmacologiche Mario Negri, IRCCS, Milan 20156, Italy;* orcid.org/0000-0002-2152-6517; Email: luisa.decola@unimi.it

Authors

Alessia Lucrezia Fenaroli − *Department of Biochemistry and Molecular Pharmacology, Istituto di Ricerche Farmacologiche Mario Negri, IRCCS, Milan 20156, Italy*

Mirco Scaccaglia − *Department of Biochemistry and Molecular Pharmacology, Istituto di Ricerche Farmacologiche Mario Negri, IRCCS, Milan 20156, Italy;* orcid.org/0000-0001-9232-8772

Cristina Matteo − *Department of Oncology, Laboratory of Cancer Pharmacology, Istituto di Ricerche Farmacologiche Mario Negri, IRCCS, Milan 20156, Italy*

Chiara Grasselli − *Department of Oncology, Immunopharmacology Unit, Istituto di Ricerche Farmacologiche Mario Negri, IRCCS, Milan 20156, Italy*

Massimo Zucchetti − *Department of Oncology, Laboratory of Cancer Pharmacology, Istituto di Ricerche Farmacologiche Mario Negri, IRCCS, Milan 20156, Italy*

Roberta Frapolli − *Department of Oncology, Laboratory of Cancer Pharmacology, Istituto di Ricerche Farmacologiche Mario Negri, IRCCS, Milan 20156, Italy;* orcid.org/0000-0003-2907-273X

Claudia Nastasi − *Department of Oncology, Immunopharmacology Unit, Istituto di Ricerche Farmacologiche Mario Negri, IRCCS, Milan 20156, Italy*

Complete contact information is available at: https://pubs.acs.org/10.1021/acsomega.4c02838

Author Contributions

¶M.S.A. and A.F. contributed equally.

Author Contributions

●C.N. and L.D.C. contributed equally.

Funding

This project has received funding from the European Union's Horizon 2020 research and innovation program under grant agreement (FET-Open No 964386), project acronym "MimicKEY". M. S.-A. thanks the AIRC-Foundation for a Postdoctoral fellowship in Italy (26907-2021) and the AECC for postdoctoral research fellowship funding (POST-D234966SANC), "Ayuda a Talento AECC 2023". C.N. is supported by Fondazione Beppe e Nuccy Angiolini Onlus.

Notes

The authors declare no competing financial interest.

■ ACKNOWLEDGMENTS

We kindly thank Dr. Victor Sebastian for the electronic microscopy images performed in the LMA and in the INMA from the University of Zaragoza. We also thank the LMA for the energy-dispersive X-ray spectroscopy analysis (EDS). Alessandro Corbelli and Fabio Fiordaliso of the Mario Negri Institute for Pharmacological Research are acknowledged for some TEM images. We thank the University of Milan for the support of the APC central fund.

■ ABBREVIATIONS

CIT, chemoimmunotherapy; DOX, doxorubicin; NPs, nanoparticles; ssOSCs, organosilica nanocages; ssMSNs, mesoporous organosilica nanoparticles; PEG, poly(ethylene)glycol

■ REFERENCES

(1) Siegel, R. L.; Miller, K. D.; Wagle, N. S.; Jemal, A. Cancer statistics, 2023. *CA. Cancer J. Clin.* **2023**, *73*, 17−48.
(2) Lawler, M.; et al. The Lancet Oncology Commission European Groundshot — addressing Europe ' s cancer research challenges : a Lancet Oncology Commission. *Lancet Oncol. Comm.* **2023**, *24*, e11−56.
(3) Han, C.; Zhan, Q. Precision medicine revolutionizes cancer diagnosis and treatment. *Med. Rev.* **2023**, *2*, 541−543.
(4) Parab, A.; Kumar Bhatt, L.; Omri, A. Targeting Epigenetic Mechanisms: A Boon for Cancer Immunotherapy. *Biomedicines* **2023**, *11*, 169.
(5) Kargbo, R. B. Effective Combination Therapies for the Treatment of HER2 Cancer. *ACS Med. Chem. Lett.* **2023**, *14*, 231−232.
(6) Vanneman, M.; Dranoff, G. Combining immunotherapy and targeted therapies in cancer treatment. *Nat. Rev. Cancer* **2012**, *12*, 237−251.
(7) Emens, L. A. Chemoimmunotherapy. *Cancer J.* **2010**, *16*, 295−303.
(8) Fujimoto, D.; et al. Outcomes of Chemoimmunotherapy Among Patients With Extensive-Stage Small Cell Lung Cancer According to Potential Clinical Trial Eligibility. *JAMA Netw. Open* **2023**, *6*, e230698−e230698.
(9) Akao, T.; et al. A poly(gamma-glutamic acid)-amphiphile complex as a novel nanovehicle for drug delivery system. *J. Drug Target.* **2010**, *18*, 550−556.
(10) Akkın, S.; Varan, G.; Bilensoy, E. A Review on Cancer Immunotherapy and Applications of Nanotechnology to Chemo-immunotherapy of Different Cancers. *Molecules* **2021**, *26*, 3382.
(11) Mu, W.; Chu, Q.; Liu, Y.; Zhang, N. A Review on Nano-Based Drug Delivery System for Cancer Chemoimmunotherapy. *Nano-micro Lett.* **2020**, *12*, 142.
(12) Gao, Y.; Gao, D.; Shen, J.; Wang, Q. A Review of Mesoporous Silica Nanoparticle Delivery Systems in Chemo-Based Combination Cancer Therapies. *Front. Chem.* **2020**, *8*, No. 598722.
(13) Yang, Y.; et al. Hybrid Nanoreactors: Enabling an Off-the-Shelf Strategy for Concurrently Enhanced Chemo-immunotherapy. *Angew. Chemie Int. Ed.* **2018**, *57*, 11764−11769.
(14) Kong, M.; et al. Biodegradable Hollow Mesoporous Silica Nanoparticles for Regulating Tumor Microenvironment and Enhancing Antitumor Efficiency. *Theranostics* **2017**, *7*, 3276−3292.
(15) Qian, G.; et al. An immuno-potentiating vehicle made of mesoporous silica-zinc oxide micro-rosettes with enhanced doxorubicin loading for combined chemoimmunotherapy. *Chem. Commun. (Camb).* **2019**, *55*, 961−964.
(16) Feng, X.; et al. TRAIL-modified, doxorubicin-embedded periodic mesoporous organosilica nanoparticles for targeted drug delivery and efficient antitumor immunotherapy. *Acta Biomater.* **2022**, *143*, 392−405.
(17) Wang, S.; et al. Amelioration of systemic antitumor immune responses in cocktail therapy by immunomodulatory nanozymes. *Sci. Adv.* **2022**, *8*, No. eabn3883.
(18) Sancho-Albero, M.; et al. Enhancing Pt (IV) Complexes Anticancer Activity Upon Encapsulation in Stimuli Responsive Nanocages. *Adv. Healthc. Mater.* **2023**, *12*, No. 2202932.
(19) Talamini, L.; et al. Organosilica Cages Target Hepatic Sinusoidal Endothelial Cells Avoiding Macrophage Filtering. *ACS Nano* **2021**, *15*, 9701−9716.
(20) Prasetyanto, E. A.; et al. Breakable Hybrid Organosilica Nanocapsules for Protein Delivery. *Angew. Chem., Int. Ed. Engl.* **2016**, *55*, 3323−3327.
(21) Maggini, L.; et al. Breakable mesoporous silica nanoparticles for targeted drug delivery. *Nanoscale* **2016**, *8*, 7240−7247.
(22) Picchetti, P. Smart Nanocages as a Tool for Controlling Supramolecular Aggregation. *J. Am. Chem. Soc.* **2021**, *143*, 7681.
(23) Ma, K.; et al. Self-assembly of highly symmetrical, ultrasmall inorganic cages directed by surfactant micelles. *Nature* **2018**, *558*, 577−580.
(24) Aubert, T.; Huang, J.-Y.; Ma, K.; Hanrath, T.; Wiesner, U. Porous cage-derived nanomaterial inks for direct and internal three-dimensional printing. *Nat. Commun.* **2020**, *11*, 4695.
(25) Li, Y.; Kröger, M.; Liu, W. K. Endocytosis of PEGylated nanoparticles accompanied by structural and free energy changes of the grafted polyethylene glycol. *Biomaterials* **2014**, *35*, 8467−8478.
(26) Canton, I.; Battaglia, G. Endocytosis at the nanoscale. *Chem. Soc. Rev.* **2012**, *41*, 2718−2739.
(27) Yue, Z.-G.; et al. Surface charge affects cellular uptake and intracellular trafficking of chitosan-based nanoparticles. *Biomacromolecules* **2011**, *12*, 2440−2446.
(28) Pestka, J.; Zhou, H.-R. Toll-Like Receptor Priming Sensitizes Macrophages to Proinflammatory Cytokine Gene Induction by Deoxynivalenol and Other Toxicants. *Toxicol. Sci.* **2006**, *92*, 445−455.
(29) Zhou, J.; et al. The TLR7/8 agonist R848 optimizes host and tumor immunity to improve therapeutic efficacy in murine lung cancer. *Int. J. Oncol.* **2022**, *61*, 81.
(30) Rodell, C. B.; et al. TLR7/8-agonist-loaded nanoparticles promote the polarization of tumour-associated macrophages to enhance cancer immunotherapy. *Nat. Biomed. Eng.* **2018**, *2*, 578−588.
(31) Anfray, C. Intratumoral combination therapy with poly(I:C) and resiquimod synergistically triggers tumor-associated macrophages for effective systemic antitumoral immunity. *J. Immunother. Cancer* **2021**, *9*, e002408.
(32) Liu, Y.; et al. All-Trans Retinoic Acid and Doxorubicin Delivery by Folic Acid Modified Polymeric Micelles for the Modulation of Pin1-Mediated DOX-Induced Breast Cancer Stemness and Metastasis. *Mol. Pharmaceutics* **2021**, *18*, 3966−3978.
(33) Rong, Y.; et al. Doxorubicin resistant cancer cells activate myeloid-derived suppressor cells by releasing PGE2. *Sci. Rep.* **2016**, *6*, 23824.

https://doi.org/10.1021/acsomega.4c02838
ACS Omega 2024, 9, 41225−41235